Quantifying and Managing Uncertainty in Operational Modal Analysis

Siu-Kui Au[*1], James M.W. Brownjohn[2] and John E. Mottershead[1]

[1]Center for Engineering Dynamics and Institute for Risk and Uncertainty, University of Liverpool

[2]College of Engineering, Mathematics & Physical Sciences, University of Exeter

Abstract

Operational modal analysis aims at identifying the modal properties (natural frequency, damping, etc.) of a structure using only the (output) vibration response measured under ambient conditions. Highly economical and feasible, it is becoming a common practice in full-scale vibration testing. In the absence of (input) loading information, however, the modal properties have significantly higher uncertainty than their counterparts identified from free or forced vibration (known input) tests. Mastering the relationship between identification uncertainty and test configuration is of great interest to both scientists and engineers, e.g., for achievable precision limits and test planning/budgeting. Addressing this challenge beyond the current state-of-the-art that are mostly concerned with identification algorithms, this work obtains closed form analytical expressions for the identification uncertainty (variance) of modal parameters that fundamentally explains the effect of test configuration. Collectively referred as 'uncertainty laws', these expressions are asymptotically correct for well-separated modes, small damping and long data; and are applicable under non-asymptotic situations. They provide a scientific basis for planning and standardization of ambient vibration tests, where factors such as channel noise, sensor number and location can be quantitatively accounted for. The work is reported comprehensively with verification through synthetic and experimental data (laboratory and field), scientific implications and practical guidelines for planning ambient vibration tests.

[*] Corresponding author. E-mail: siukuiau@liverpool.ac.uk. Office phone: +44 (0)151 794 5217

Keywords:

Ambient vibration test; asymptotics; BAYOMA; operational modal analysis; signal-to-noise ratio; uncertainty law

1. Introduction

Operational modal analysis (OMA) aims at identifying the modal properties (natural frequency, damping ratio, mode shape, etc) of a constructed structure using only the (output) vibration response (acceleration, velocity, etc) [1][2][3]. The (input) excitation to the structure is not measured but is assumed to be broadband random. This allows vibration data to be collected when the structure is in its working or 'operational' condition without much intervention. This implies significant economy in implementation, which to a large extent has contributed to the increasing popularity of OMA in practical applications [4][5][6][7].

In the absence of loading information, the identification uncertainty of modal parameters from ambient vibration data is significantly higher than that in free vibration or force vibration tests. This is complicated by variability due to modeling errors regarding the stationary or broadband nature of loading, and the effects of structural/environmental changes [8][9][10]. Uncertainty quantification and quality control on the identified modal properties therefore become especially relevant. From a scientific point of view, it is of interest to know what factors the identification uncertainty depends on and what the relationship is. For planning or specification purposes, it is desirable to have an assessment of the identification uncertainty for a given test configuration. For example, how long should the data be? How many sensors are required? Should better sensors be used? These are long-standing issues that have presented challenges to researchers and practitioners [11][12][13][14].

A Bayesian approach provides a fundamental basis for extracting the information contained in the data for inferring the parameters of interest in a manner consistent with probability and modeling assumptions [15][16][17]. In OMA this has recently been materialized and put into practice, where making inference based on the 'raw' FFT (i.e.,

no filtering, windowing, etc.) within a selected frequency band is found to yield a computationally efficient method whose modeling assumptions are robust to applications. See [18] for the first formulation, [19] for a recent review and [20][21][22][23][24] for examples of recent applications. In a Bayesian context, identification results are encapsulated in the joint 'posterior' (i.e., given data) distribution of the modal parameters. With sufficient data often encountered in applications, the posterior distribution has a single peak and it can be approximated by a Gaussian distribution. The mean of the Gaussian distribution gives the posterior most probable value (MPV) of the modal parameters, while the covariance matrix reflects their remaining identification uncertainty. In a non-Bayesian, or 'frequentist' context, identification uncertainty has been defined as the ensemble variance of estimates over repeated experiments. Methods of calculation based on perturbation have been developed in [25][26][27] for time-domain state-space models. See also [28] that investigated empirically the effects of various sources on identification results.

Being able to calculate the identification uncertainty for a given set of data alone does not provide much insight about how it depends on test configuration. Due to complexity of the problem, the exact dependence is expected to be complicated and is unlikely to be described in a closed-form explicit manner. Motivated by observations on the identification uncertainty of modal parameters in terms of their posterior c.o.v. (coefficient of variation = standard deviation / mean) monitored during typhoons, an asymptotic analysis has been performed for the posterior covariance matrix [29]. Focusing on well-separated modes, the study yielded closed-form expressions for the leading (zeroth) order of the posterior c.o.v. under the asymptotic condition of small damping and long data duration. The results were collectively referred as 'uncertainty laws', analogous to the laws of large numbers in statistics. They were found to be remarkably simple and insightful.

The theory of uncertainty laws motivated the definition of the 'modal signal-to-noise (s/n) ratio' as the PSD (power spectral density) ratio of the modal response to noise at the natural frequency. This was found to be the only parameter in the uncertainty laws that

reflects test configuration attributes such as instrument noise, the number of sensors and their locations. However, the leading (zeroth) order of the uncertainty laws obtained so far does not depend on the modal s/n ratio. In this sense the zeroth order expression gives the 'achievable precision limit' when the modal s/n ratio is infinite. The objective of this work is to further capture the effect of the modal s/n ratio in the uncertainty laws so that test configuration can be quantified for planning or standardizing ambient vibration tests. To achieve this objective, we perform a first order asymptotic analysis of the posterior c.o.v.s, leading to 'first order uncertainty laws'.

This work is organized as follow. We first give a short overview of the Bayesian framework for OMA, based on which the uncertainty laws were derived. The zeroth order laws will then be reviewed. The key results of the first order laws will be summarized, followed by an outline of derivation with details referred to the appendix. The first order laws will be verified and their approximation under non-asymptotic conditions will be investigated using synthetic data and experimental data. Implications and applications of the uncertainty laws for planning ambient vibration tests will also be discussed.

2. Bayesian framework

Let the acceleration time history at n measured DOFs of a structure be $\{\hat{\ddot{\mathbf{x}}}_j \in R^n\}_{j=0}^{N-1}$ and abbreviated as $\{\hat{\ddot{\mathbf{x}}}_j\}$, where N is the number of samples per data channel. The (scaled one-sided) FFT of $\{\hat{\ddot{\mathbf{x}}}_j\}$ is the complex-valued sequence $\{\mathcal{F}_k \in C^n\}_{k=0}^{N-1}$ where

$$\mathcal{F}_k = \sqrt{\frac{2\Delta t}{N}} \sum_{j=0}^{N-1} \hat{\ddot{\mathbf{x}}}_j e^{-2\pi \mathbf{i} jk/N} \tag{1}$$

$\mathbf{i}^2 = -1$ and Δt is the sampling interval. For a given k, the FFT $\mathcal{F}_k$ corresponds to the frequency $\mathrm{f}_k = k/N\Delta t$, up to the Nyquist frequency.

As in the conventional setting, consider a classically damped mode well-separated from other modes. It is identified using only the $\mathcal{F}_k$ s on a selected band near the natural frequency. In the band it is assumed that $\mathcal{F}_k = \boldsymbol{\Phi}\ddot{\eta}_k + \boldsymbol{\varepsilon}_k$ where $\boldsymbol{\Phi} \in R^n$ is the mode shape confined to the measured DOFs (scaled to have unit Euclidean norm, i.e., $\| \boldsymbol{\Phi} \|^2 = \boldsymbol{\Phi}^T \boldsymbol{\Phi} = 1$); $\boldsymbol{\varepsilon}_k \in C^n$ is the FFT of channel noise; and $\ddot{\eta}_k \in C$ is the FFT of the modal acceleration response whose time domain counterpart satisfies $\ddot{\eta}(t) + 2\zeta\omega\dot{\eta}(t) + \omega^2\eta(t) = p(t)$. Here $\omega = 2\pi f$ (rad/sec), f is the natural frequency (in Hz), ζ is the damping ratio and $p(t)$ is the modal force. The modal force and channel noise are assumed to have a constant PSD within the selected band, denoted respectively by S and S_e. In the above context, the set of modal parameters to be identified is $\boldsymbol{\theta} = \{f, \zeta, S, S_e, \boldsymbol{\Phi}\}$.

Let $\{\mathcal{F}_k\}$ denote the collection of FFT data within the selected band. Using Bayes' Theorem with a uniform prior distribution for $\boldsymbol{\theta}$, the posterior PDF can be written as $p(\boldsymbol{\theta} \mid \{\mathcal{F}_k\}) \propto \exp[-L(\boldsymbol{\theta})]$ where

$$L(\boldsymbol{\theta}) = -\ln p(\{\mathcal{F}_k\} \mid \boldsymbol{\theta}) = nN_f \ln \pi + \sum_k \ln |\mathbf{E}_k| + \sum_k \mathcal{F}_k^* \mathbf{E}_k^{-1} \mathcal{F}_k \qquad (2)$$

is called the negative log-likelihood function (NLLF); $\mathbf{E}_k = SD_k \overline{\boldsymbol{\Phi}}\overline{\boldsymbol{\Phi}}^T + S_e \mathbf{I}_n$ is the theoretical PSD matrix of data for given $\boldsymbol{\theta}$; $\overline{\boldsymbol{\Phi}} = \| \boldsymbol{\Phi} \|^{-1} \boldsymbol{\Phi}$ and

$$D_k(f, \zeta) = [(1 - \beta_k^2)^2 + (2\zeta\beta_k)^2]^{-1} \qquad (\beta_k = f / \mathrm{f}_k) \qquad (3)$$

is the dynamic amplification factor. The expression of the likelihood function stems from the standard result in signal processing that for long data duration the FFTs of a stationary stochastic process are asymptotically independent at different frequencies and jointly complex Gaussian [31]. For computational purpose, the following equivalent form that reveals a quadratic dependence on $\overline{\boldsymbol{\Phi}}$ is used [32]:

$$L(\boldsymbol{\theta}) = nN_f \ln \pi + (n-1)N_f \ln S_e + \sum_k \ln(SD_k + S_e) + S_e^{-1}(d - \overline{\boldsymbol{\Phi}}^T \mathbf{A} \overline{\boldsymbol{\Phi}}) \qquad (4)$$

$$\mathbf{A} = \sum_k (1 + \frac{S_e}{SD_k})^{-1} \mathbf{D}_k \qquad \mathbf{D}_k = \mathrm{Re}[\mathcal{F}_k \mathcal{F}_k^*] \qquad d = \sum_k \mathcal{F}_k^* \mathcal{F}_k \qquad (5)$$

The uncertainty laws of well-separated modes are derived based on the above identification framework.

3. Zeroth order laws

For well-separated modes, small damping and sufficiently long data duration, closed form expressions for the leading order of the posterior c.o.v.s of modal parameters have been derived [29], referred as the 'zeroth order laws' in this work. Specifically, suppose the selected band is $f(1 \pm \kappa\zeta)$, where κ is called the 'bandwidth factor' that reflects the amount of usable (frequency-domain) information in the data for identifying the mode, often a trade-off between identification precision and modeling error risk. Let T_d be the data duration. Since the frequency spacing is T_d^{-1}, there are $N_f = 2\kappa\zeta f / T_d^{-1} = 2\kappa\zeta N_c$ FFT ordinates in the band $f(1 \pm \kappa\zeta)$, where $N_c = T_d f$ is the 'normalized data length' as a multiple of the natural period. The above definitions are illustrated in Figure 1, which shows an idealized singular value spectrum, i.e., plot of the eigenvalues of acceleration data PSD matrix with frequency. In the resonance band of a mode, the largest eigenvalue is equal to $SD_k + S_e$ and the remaining ones are all S_e.

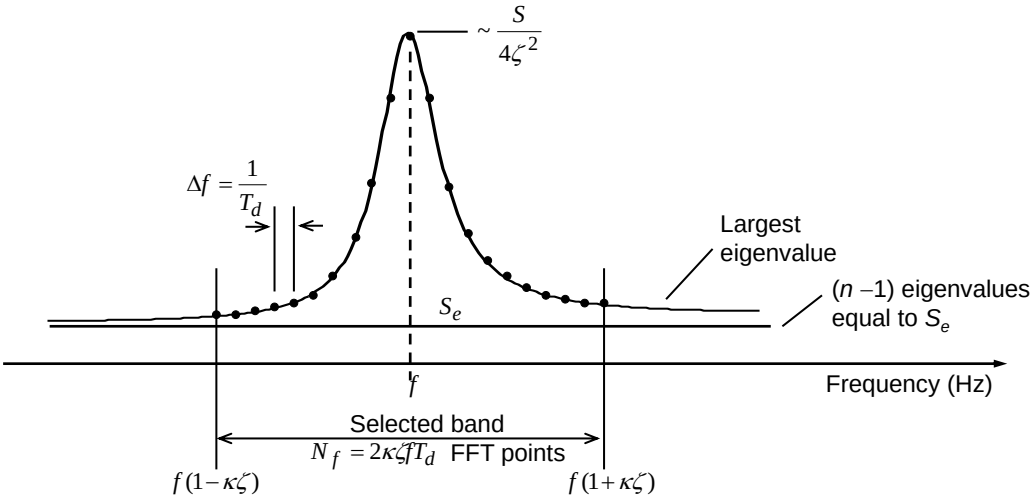

Figure 1 Idealized singular value spectrum of acceleration data in a band dominated by a single mode with frequency f and damping ratio ζ

In the above context, for small damping ζ and large N_f, the leading (zeroth) order of the posterior c.o.v.s of f, ζ, S are given respectively by (the subscript '0' denotes 'zeroth order')

$$\delta_{f0}^2 = \frac{\zeta}{2\pi N_c B_f} \qquad \delta_{\zeta 0}^2 = \frac{1}{2\pi\zeta N_c B_\zeta} \qquad \delta_{S0}^2 = \frac{1}{N_f B_S} \tag{6}$$

where

$$B_f(\kappa) = \frac{2}{\pi}(\tan^{-1}\kappa - \frac{\kappa}{\kappa^2+1}) \tag{7}$$

$$B_\zeta(\kappa) = \frac{2}{\pi}\left[\tan^{-1}\kappa + \frac{\kappa}{\kappa^2+1} - \frac{2(\tan^{-1}\kappa)^2}{\kappa}\right] \tag{8}$$

$$B_S(\kappa) = 1 - 2(\tan^{-1}\kappa)^2\kappa^{-1}(\tan^{-1}\kappa + \frac{\kappa}{\kappa^2+1})^{-1} \tag{9}$$

are 'data length factors' reflecting that only a limited bandwidth is used for modal identification. The data length factors increase monotonically with κ and range between 0 and 1. The posterior covariance matrix for the mode shape is asymptotically given by

$$\mathbf{C}_\Phi \sim \frac{2\nu\zeta}{\pi N_c B_\Phi(\kappa)}(\mathbf{I}_n - \overline{\mathbf{\Phi}}\overline{\mathbf{\Phi}}^T) \tag{10}$$

where

$$\nu = \frac{S_e}{S} \tag{11}$$

is the 'noise-to-environment' (n/e) ratio; and $B_\Phi(\kappa) = (2/\pi)\tan^{-1}\kappa$ is the data length factor for mode shape. In presenting the uncertainty laws, modal parameter symbols such as f and ζ denote the actual property of the structure that gives the data. This should be distinguished from those in the NLLF that represent variables in a Bayesian inference problem.

4. First order laws (main theoretical results)

One important aspect of the zeroth order laws is that they do not depend on test configuration attributes such as channel noise or sensors (number and location). Essentially, the zeroth order laws give the identification uncertainty when the s/n ratio is infinitely high because the damping ratio is taken to be asymptotically small. The objective of this work is to further capture the effect of test configuration. The Bayesian OMA framework [19] and a first order asymptotic analysis of posterior uncertainty motivated the definition of the 'modal s/n ratio' as the PSD ratio of modal response ($S/4\zeta^2$) to noise (S_e) at the natural frequency:

$$\gamma = \frac{S}{4S_e\zeta^2} \tag{12}$$

This is approximately equal to the ratio of the largest to the second largest eigenvalue of the data PSD matrix at the natural frequency (Figure 1).

The modal s/n ratio turns out to be the only parameter in the uncertainty laws that carries the influence of test configuration.

We show that the posterior c.o.v. δ_x of modal parameter x $(= f, \zeta, S)$ is given by, to the first order of the small parameter γ^{-1} as $\zeta \to 0$ and $N_f \to \infty$,

$$\delta_x^2 \sim \delta_{x1}^2 = \delta_{x0}^2(1 + a_x\gamma^{-1}) \qquad x = f, \zeta, S \tag{13}$$

where

$$a_f(\kappa) = \frac{4(\kappa - \tan^{-1}\kappa)}{\tan^{-1}\kappa - \dfrac{\kappa}{\kappa^2+1}} \tag{14}$$

$$a_\zeta(\kappa) = \frac{4(\kappa^2+1)(3\tan^{-1}\kappa - 3\kappa + \kappa^2\tan^{-1}\kappa)\tan^{-1}\kappa}{3[(\kappa^2+1)(\kappa - 2\tan^{-1}\kappa)\tan^{-1}\kappa + \kappa^2]} \tag{15}$$

$$a_S(\kappa) = 2 + \frac{2}{3}\kappa^2 - \frac{(\tan^{-1}\kappa)^2}{2(\tan^{-1}\kappa)^2 - b\kappa}\left[\frac{8\tan^{-1}\kappa}{b} - \frac{8\kappa}{\tan^{-1}\kappa} + \frac{4}{3}\kappa^2 + 4\right] \tag{16}$$

are 'first order coefficients'; and $b = \tan^{-1}\kappa + \kappa/(\kappa^2+1)$.

Equations (13) is a first order asymptotic expression in the following sense:

$$\frac{\delta_x^2}{\delta_{x0}^2} = 1 + a_x\gamma^{-1} + O(\gamma^{-2}) \qquad \text{as } \zeta \to 0, N_f \to \infty \qquad x = f, \zeta, S \qquad (17)$$

The term $a_x\gamma^{-1}$ captures the first order effect with respect to (w.r.t.) γ^{-1}. It tends to zero as $\zeta \to 0$ (hence $\gamma \to \infty$) but it captures the primary effect of γ when γ is not high. The first order uncertainty law for S_e is not presented as it is of little practical interest. For the mode shape, the effect of γ is already contained in the zeroth order law in (10).

5. Quantification of test configuration

The zeroth order laws give the achievable limit of OMA modal parameter identification precision when the modal s/n ratio γ is infinite. They are primarily influenced by the structure and data length, and less by test configuration. The first order laws capture the effect of finite γ, which carries the influence of test configuration. It is remarkable that the apparently complicated influence of test configuration can be fundamentally quantified in a simple manner though γ, even though this is only asymptotically correct for small damping and long data.

The modal s/n ratio depends on the channel noise PSD S_e, the damping ratio ζ and the modal force PSD S. The modal force PSD depends on the intensity of environmental excitation. It also depends on the measured DOFs in a less trivial manner, which turns out to be the only means by which the measured DOFs affect identification uncertainty as implied by the uncertainty laws. Specifically, let $\boldsymbol{\xi}$ denote the full mode shape of the structure, i.e., containing all (possibly an infinite number of) DOFs. The modal force PSD corresponding to the scaling implied by $\boldsymbol{\xi}$ is

$$S_p = \frac{\boldsymbol{\xi}^T \mathbf{S}_F \boldsymbol{\xi}}{(\boldsymbol{\xi}^T \mathbf{M} \boldsymbol{\xi})^2} \qquad (18)$$

where $\mathbf{S}_F$ is the PSD matrix of applied forces and $\mathbf{M}$ is the mass matrix. In reality $\boldsymbol{\xi}$ can hardly be identified because of limited measured DOFs, and so is S_p. Without loss of generality, assume that the first n DOFs of $\boldsymbol{\xi}$ are measured and the measured mode shape is scaled to have unit norm, as in the Bayesian OMA framework. Under this scaling, $\boldsymbol{\xi}$ should be divided by $\sqrt{\sum_{i=1}^{n}\xi_i^2}$. Replacing $\boldsymbol{\xi}$ in (18) by $\boldsymbol{\xi}/\sqrt{\sum_{i=1}^{n}\xi_i^2}$ gives the modal force PSD under the new scaling:

$$S = S_p \sum_{i=1}^{n} \xi_i^2 \tag{19}$$

This is the quantity that can be identified from data with limited measured DOFs. Equation (19) implies that increasing the number of measured DOFs always increases S and hence the modal s/n ratio. The rate of increase depends on the mode shape value of the DOF incrementally added to the existing set of measured DOFs. See an illustration in Section 7.2 later.

6. Outline of derivation

In this section we outline the derivation of the first order uncertainty laws, where details are referred to the appendix. First recall from [29] that, to the leading order, the posterior c.o.v.s are given by

$$\delta_f^2 \sim L^{(ff)-1} \qquad \delta_\zeta^2 \sim L^{(\zeta\zeta)-1}(1-q_{\zeta S}^2)^{-1} \qquad \delta_S^2 \sim L^{(SS)-1}(1-q_{\zeta S}^2)^{-1} \tag{20}$$

where $L^{(ff)}$, $L^{(\zeta\zeta)}$ and $L^{(SS)}$ are the second derivatives of the NLLF w.r.t. f, ζ and S, respectively, and evaluated at the MPV;

$$q_{\zeta S} = \frac{L^{(\zeta S)}}{\sqrt{L^{(\zeta\zeta)}L^{(SS)}}} \tag{21}$$

is the 'cross sensitivity coefficient' between ζ and S. Throughout this work, we use a superscripted variable to denote the derivative of the subject quantity w.r.t. that variable.

The zeroth order asymptotic expressions (denoted with a subscript '0') for the second derivatives that led to (6) were given by:

$$L_0^{(ff)} = \frac{4N_c}{f^2\zeta}(\tan^{-1}\kappa - \frac{\kappa}{\kappa^2+1}) \qquad L_0^{(\zeta\zeta)} = \frac{4N_c}{\zeta}(\tan^{-1}\kappa + \frac{\kappa}{\kappa^2+1}) \tag{22}$$

$$L_0^{(SS)} = S^{-2}N_f \qquad L_0^{(\zeta S)} = -4S^{-1}N_c\tan^{-1}\kappa \tag{23}$$

$$q_{\zeta S0}^2 = 2(\tan^{-1}\kappa)^2\kappa^{-1}(\tan^{-1}\kappa + \frac{\kappa}{\kappa^2+1})^{-1} \tag{24}$$

Since $\gamma^{-1} = 4\nu\zeta^2$, the first order effect of modal s/n ratio can be captured by retaining up to the $O(\zeta^2)$ terms in the asymptotic expressions of the posterior c.o.v.s. The first order term in the posterior c.o.v.s can be obtained in terms of those of the derivatives $L^{(ff)}$, $L^{(\zeta\zeta)}$, $L^{(SS)}$ and $L^{(f\zeta)}$. It is shown in the appendix that ($x = f, \zeta, S$)

$$L^{(xx)} \sim L_0^{(xx)}(1 - c_{xx}\gamma^{-1}) \qquad L^{(\zeta S)} \sim L_0^{(\zeta S)}(1 - c_{\zeta S}\gamma^{-1}) \tag{25}$$

where

$$c_{ff}(\kappa) = \frac{4(\kappa - \tan^{-1}\kappa)}{\tan^{-1}\kappa - \frac{\kappa}{\kappa^2+1}} \qquad c_{\zeta\zeta}(\kappa) = \frac{4\tan^{-1}\kappa}{\tan^{-1}\kappa + \frac{\kappa}{\kappa^2+1}} \tag{26}$$

$$c_{SS}(\kappa) = 2(1 + \frac{\kappa^2}{3}) \qquad c_{\zeta S}(\kappa) = \frac{2\kappa}{\tan^{-1}\kappa} \tag{27}$$

Taking natural logarithm of (21) and considering small perturbation, the first order expression for $q_{\zeta S}^2$ can be written in terms of $c_{\zeta\zeta}$, c_{SS} and $c_{\zeta S}$:

$$q_{\zeta S}^2 \sim q_{\zeta S0}^2[1 - (2c_{\zeta S} - c_{\zeta\zeta} - c_{SS})\gamma^{-1}] \tag{28}$$

Substituting (25) and (28) into (20), the first order expression for the posterior c.o.v. is given by

$$\delta_x^2 \sim \delta_{x0}^2(1 + a_x\gamma^{-1}) \qquad x = f, \zeta, S \tag{29}$$

where

$$a_f = c_{ff} \qquad a_x = c_{xx} + \frac{q_{\zeta S0}^2}{1 - q_{\zeta S0}^2}(c_{\zeta\zeta} + c_{SS} - 2c_{\zeta S}) \qquad x = \zeta, S \tag{30}$$

Substituting the expressions for c_{ff}, $c_{\zeta\zeta}$, c_{SS}, $c_{\zeta S}$ in (26)-(27) and $q_{\zeta S0}$ in (24) into (30) and simplifying gives the expressions for a_f, a_ζ and a_S in (14)-(16).

7. Verification with synthetic data

In this section we present examples with synthetic data to investigate the approximate nature of the first order uncertainty laws under non-asymptotic conditions. The examples also illustrate the effect of channel noise level and measured DOFs on the modal s/n ratio and hence on the posterior c.o.v. of modal parameters. The same structure in **[30]** is considered, when the zeroth order law was investigated.

Consider the horizontal vibration of a ten-storied shear building (i.e., with ten DOFs in total) with uniform mass of 1000 tons per floor, interstory stiffness of 1767kN/mm and damping ratio of 1% in all modes. The natural frequencies of the first three modes are 1Hz, 2.98Hz and 4.89Hz. The structure is subjected to i.i.d. white noise excitation at all floors, each with a PSD of $S_w = 96.2N^2/Hz$. Synthetic acceleration data is generated at a sampling rate of 100Hz for a duration of 600sec. The data is contaminated by i.i.d. white channel noise with a PSD of S_e (value see later).

7.1. Effect of channel noise

Consider identifying the first mode with two accelerometers placed on the fifth floor and the roof. As a reference, the modal force PSD corresponding to this sensor layout (with measured mode shape scaled to have unit norm) is calculated to be $S = 0.278(\mu g)^2/Hz$. Modal identification is based on the FFTs of the measured acceleration data on the frequency band [0.96, 1.04] Hz, corresponding to a bandwidth factor of $\kappa = 4$. Consider different data sets contaminated by channel noise of different values of PSD S_e, ranging from 500 to $1\,(\mu g)^2/Hz$. Correspondingly, the modal s/n ratio $\gamma = S/4S_e\zeta^2$ ranges

from $(0.278)/[4(500)(0.01)^2] = 1.39$ to $(0.278)/[4(1)(0.01)^2] = 695$. For each data set, the MPVs of the modal parameters are calculated using Bayesian OMA algorithm [32].

Figure 2(a) shows the posterior c.o.v. versus γ for the different cases considered. The value of γ on the x-axis is calculated using the MPVs of the modal parameters obtained in each case. The circles show the exact values of posterior c.o.v.s. The center line and dashed line show the values based on the zeroth order and first order uncertainty laws, respectively, calculated using the MPVs. Part of the discrepancy or scatter in the figures is due to the fluctuation of the MPVs calculated in each case. If the MPVs were equal to their exact parameter values then the zeroth order law (center line) would have been a straight horizontal line. It is seen from the figure that as γ increases the first order law (dashed line) and the exact value (circles) of the posterior c.o.v. decrease and converge to a constant level equal to the zeroth order law. The first order law captures the variation of the posterior c.o.v. with the modal s/n ratio. Generally, it agrees well with the exact value. As expected, the discrepancy is greater for smaller modal s/n ratios.

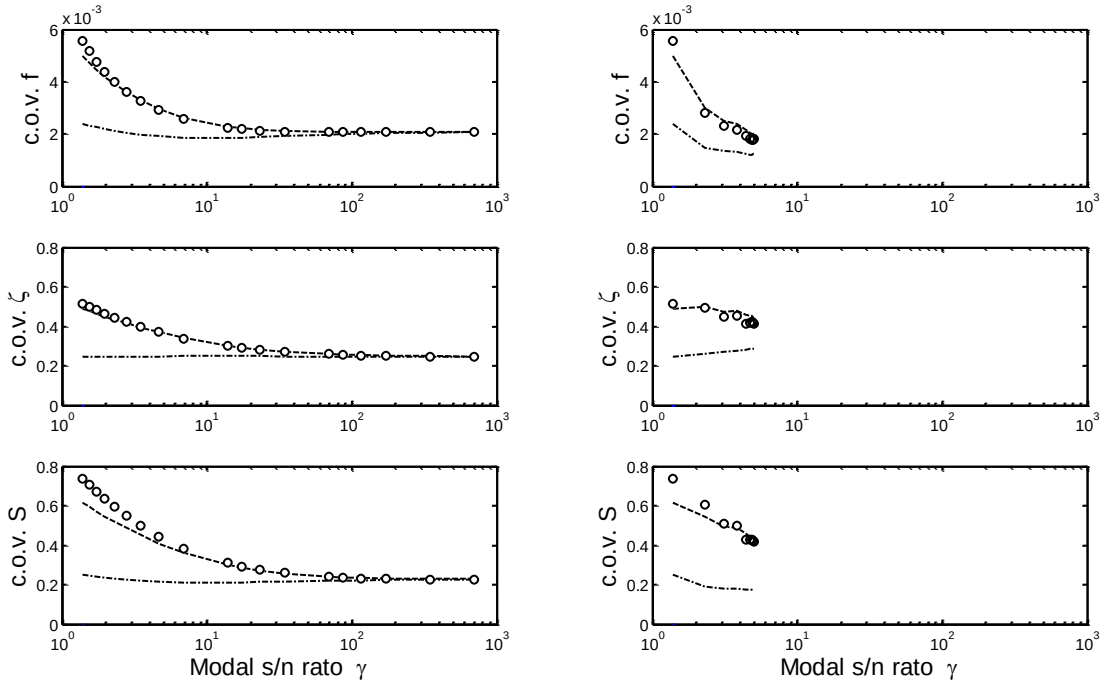

(a) Two sensors, increasing channel noise (b) Fixed channel noise, two to ten sensors

Figure 2. Posterior c.o.v. versus modal s/n ratio. Circle – exact; dashed line (- -) – first order law; center line (-.-) – zeroth order law. Uncertainty laws calculated using MPV.

7.2. Effect of measured DOFs

Suppose the channel noise level is fixed at the highest level in the last section, i.e., $S_e = 500(\mu g)^2 / Hz$. We shall investigate improving the modal s/n ratio by increasing the number of measured DOFs (each with a uniaxial accelerometer) from $n = 2$ to 10. The increasing number of sensors are placed from the top to the bottom, i.e., on the roof and 9/F for $n = 2$; on the roof, 9/F and 8/F for $n = 3$ and so on. As the number of measured DOFs increases from 2 to 10, the modal force PSD increases from $0.278(\mu g)^2 / Hz$ to $1(\mu g)^2 / Hz$. The modal s/n ratio γ increases from $(0.278)/[4(500)(0.01)^2] = 1.39$ to $(1)/[4(500)(0.01)^2] = 5$.

Figure 2(b) shows the posterior c.o.v. versus γ when the number of measured DOFs n increases from 2 to 10 in the manner just described. Since the measured DOFs are added

from the top to the bottom, the rate at which S and hence γ increases with n is decreasing because the mode shape value of the additional DOF decreases. Similar to before, the posterior c.o.v. decreases with the modal s/n ratio. The first order law (dashed line) approximates well the exact values (circles), although the discrepancy is larger for smaller modal s/n ratios. Despite the large amount of additional resources invested when the number of measured DOFs increases from 2 to 10, the posterior c.o.v. of the damping ratio only reduces from 50% to 40%, i.e., by 20%. The reduction of c.o.v. is more effective for natural frequency, by 2/3 from 0.6% to 0.2%, but this is of little significance because the c.o.v. is already very small.

8. Verification with experimental data

In this section we extend our investigation to experimental data obtained in a laboratory as well as full-scale field environment where the actual dynamics is not as well-defined and it is impossible to control the environment. These gives a real challenging test to the uncertainty laws where modeling error can exist with regard to, e.g., unaccounted modes, stationarity of response, damping mechanism, unknown colored activities. The laboratory structure is a shear frame and it will illustrate the effect of increasing measured DOFs on modal s/n ratio and hence identification uncertainty. The field structures include a footbridge and a super-tall building. The footbridge will illustrate cases with relatively low modal s/n ratios. Results of the super-tall building will be reported statistically to supplement test cases and inform the order of magnitudes of parameters in the uncertainty laws. Bayesian OMA of the above structures has been performed and so the current study provides further insights on their identification uncertainty.

As noted previously in the study of zeroth order laws, the modal s/n ratio is typically high (e.g., $\gamma > 100$) for well-managed field tests with a moderate number of servo-accelerometers. To investigate cases with low s/n ratios, we deliberately consider data sets with small modal s/n ratio, some of which can be atypical. These more challenging data sets feature higher modes, relatively high damping ratios and a small number of measured DOFs. The discrepancy between the uncertainty laws and the exact values of

posterior c.o.v. can be greater because of significant violation of the asymptotic conditions and other modeling errors associated with the identification model.

8.1. Laboratory shear frame

Consider a three-storied laboratory shear frame [33] whose measured DOFs are schematically shown in Figure 3(a). The structure was previously used to investigate a Bayesian two-stage approach for structural model identification. Ambient acceleration data was recorded for ten minutes at a sampling rate of 2048Hz and was later decimated to 512Hz for analysis. Figure 3(b) shows the root singular value spectrum calculated using the data at DOFs 1 and 2 only. The bottom line indicates roughly the root PSD level $S_e^{1/2}$ of channel noise, which ranges in the order of $100\mu g/\sqrt{Hz}$ to $20\,\mu g/\sqrt{Hz}$ from low to high frequencies. The peaks of the top line indicate potential modes. Ten well-separated modes can be recognized. Their nature are indicated, e.g., TX2 refers to the second translational mode along the x direction; R1 refers to the first torsional mode. The mode S1 near 35Hz corresponds to a torsional mode with a mode shape somewhat between R2 and R3. The frequency band used for identifying each mode is indicated by a bar below the resonance peak.

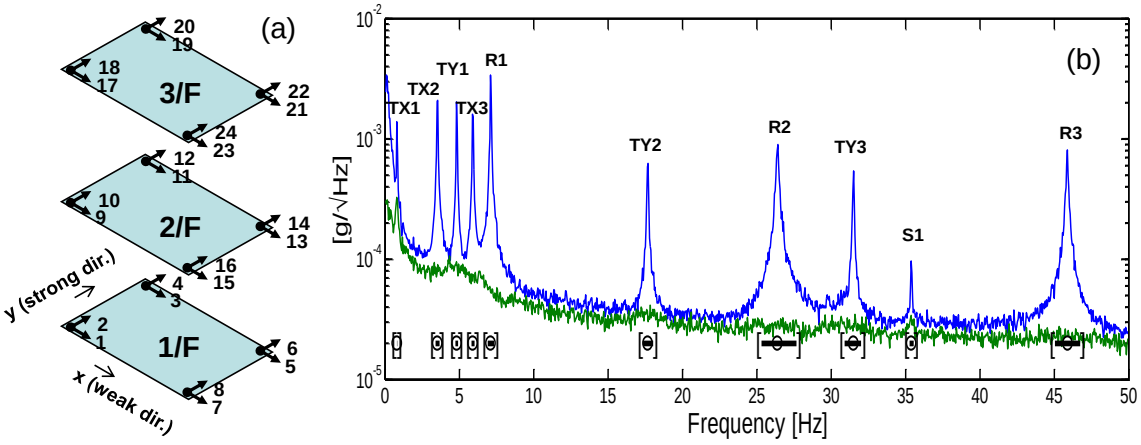

Figure 3. Laboratory frame. (a) Measured DOFs. (b) Root singular value spectrum for DOFs 1 & 2

Consider performing modal identification for Mode S1 with an increasing set of measured DOFs, starting from the smallest set with DOFs 1 and 2. This mode is chosen

for its low modal s/n ratio γ. Adding incrementally one DOF at a time, this gives for each mode 23 cases, corresponding to DOFs {1, 2}, {1, 2, 3} and so on, until {1, 2, …, 24}. Figure 4(a) shows the ratio of the posterior c.o.v. to the zeroth order law. The ratio to the zeroth order law rather than the absolute values are plotted to remove spurious fluctuations in the trend with γ due to fluctuations in the MPVs. The circles show the ratio of the exact to the zeroth order law. The crosses show the ratio of the first order law to the zeroth order law. There are 23 crosses in the figure, corresponding to 23 different sets of measured DOFs with their number increasing from $n = 2$ (DOFs 1 and 2) to $n = 24$ (all DOFs). As evidenced from the abscissas of the plots, when the number of measured DOFs increases the modal s/n ratio increases from about 20 to 400. Correspondingly, the posterior c.o.v. decreases. Ideally, if the first order law were exact and if the calculated MPVs were the same in different cases of measured DOFs, at each value of γ the cross (first order/zeroth order) should coincide with the circle (exact/zeroth order). As seen in the plots, they are generally quite close, showing a good approximation in this case. Both the crosses and circles converge to 1 for high γ. The former results directly from the uncertainty law formulas because the first order correction vanishes for high γ. The latter (circle) shows that the zeroth order law is a good approximation of the exact posterior c.o.v. for high γ, which has been verified previously .

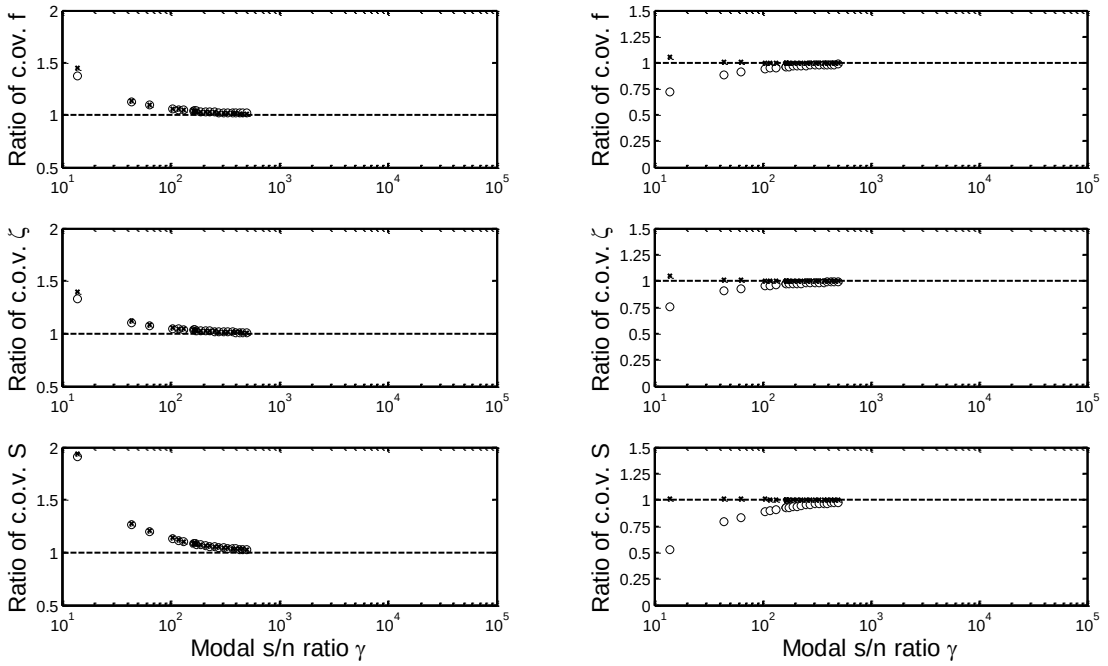

(a) Posterior c.o.v./zeroth order law (b) Posterior c.o.v./exact

Figure 4. Ratio of posterior c.o.v., lab frame, 2 to 24 DOFs, Mode S1. (a) Exact/Zeroth order (circle) and 1st order/Zeroth order (cross); (b) Zeroth order/exact (circle) and 1st order/exact (cross)

Figure 4(b) plots the ratio of the uncertainty laws to the exact values. This plot is shown to further assess the accuracy of the uncertainty laws. Ideally if the first order law were exact and the calculated MPVs were the same in different cases then the crosses should all lie on the dashed line at 1. It can be seen that the crosses are all close to 1, showing that the first order laws can provide a good approximation even when the modal s/n ratio γ is not high. On the other hand, the difference between the circles (zeroth order law) and the dashed line increases as γ decreases because the zeroth order law does not account for the effect of γ.

Figure 5 shows the results for all the ten modes indicated in Figure 3. There are $23\times10=230$ pairs of crosses and circles in the figure. Many modes have a high γ even with the smallest number of measured DOFs ($n=2$). Their results cluster in the regime $\gamma>10^4$ where the ratios are all close to 1, providing verification of the zeroth order law.

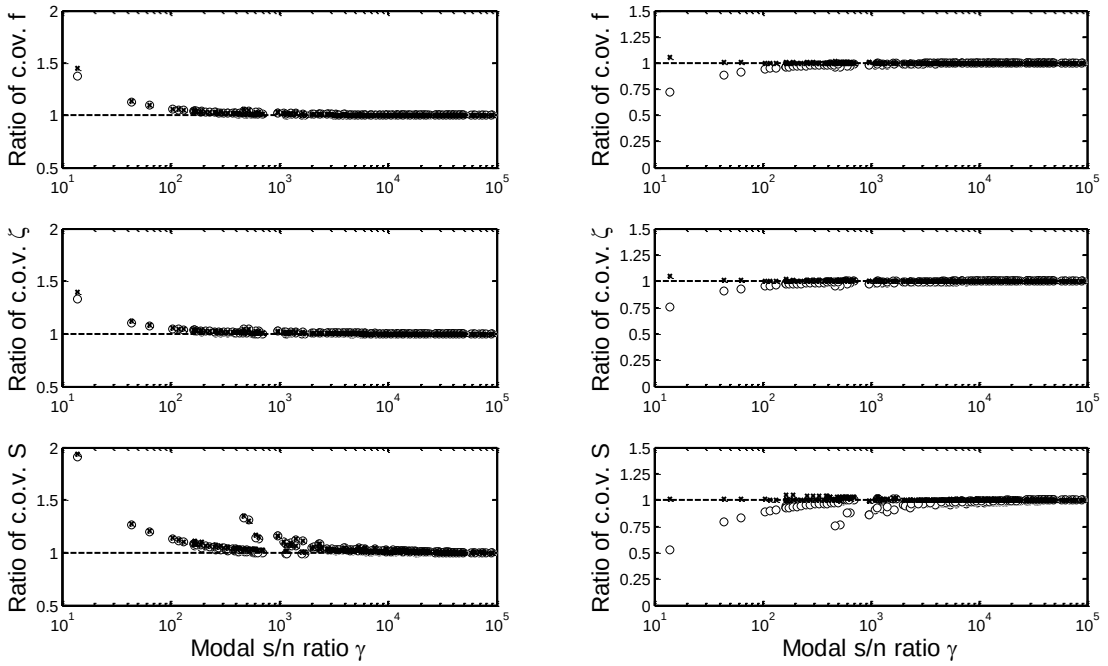

(a) Posterior c.o.v./zeroth order law (b) Posterior c.o.v./exact

Figure 5. Ratio of posterior c.o.v., lab frame, 2 to 24 DOFs, 10 modes. Same legend as Figure 4

8.2. Footbridge

Consider a multi-span footbridge measuring 12 m in width and 220 m in total length **[34]**[35]. The structure was previously used to investigate a Bayesian OMA method that can incorporate data from multiple setups. Seventy four locations distributed on two sides of the bridge were covered by thirty seven setups. Four triaxial servo-accelerometers were available and so only four locations could be measured in one setup. In all setups, two reference locations, Ref. 1 on the middle span and Ref. 2 on the side span, were always measured (each with one triaxial accelerometer). The other two accelerometers roved over the remaining locations in different setups. In each setup, five minutes of ambient acceleration data at $4\times3=12$ DOFs were collected at a sampling rate of 200Hz.

The data sets considered here correspond to the three DOFs (x, y, z) of the tri-axial accelerometer placed at Ref. 2. **Figure 6** shows the root PSD calculated using a typical

data set (the first setup). The study here focuses on the three modes that have been studied previously, whose frequency bands are indicated in the figure. These modes (in ascending order of frequency) correspond to the lateral, vertical symmetric bending and vertical asymmetric bending of the bridge, whose mode shapes are shown in **Figure 7**. From **Figure 6**, the resonance peak of Mode 3 is less pronounced compared to that of Mode 1 or Mode 2, suggesting that Mode 3 has a relatively low modal s/n ratio. In fact it is the mode that presented challenge in mode shape assembly using non-Bayesian methods, as reported in **[34]**.

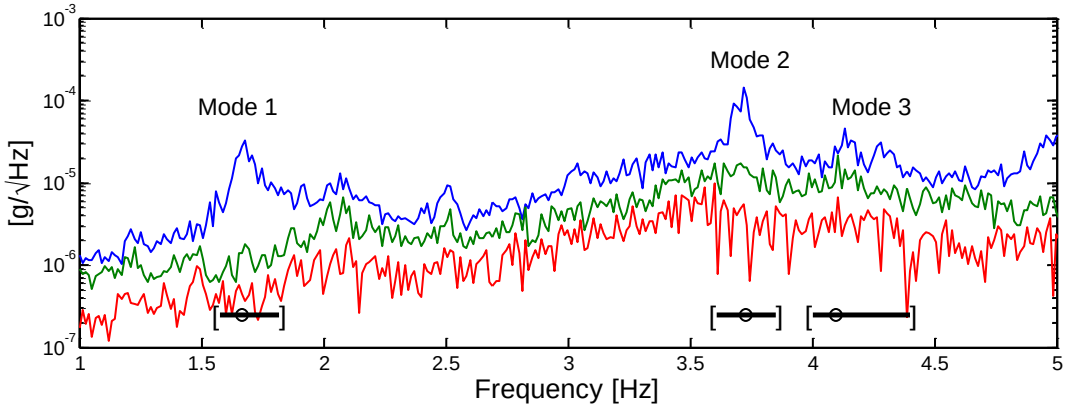

Figure 6. (Root) Singular value spectrum of a typical field data set

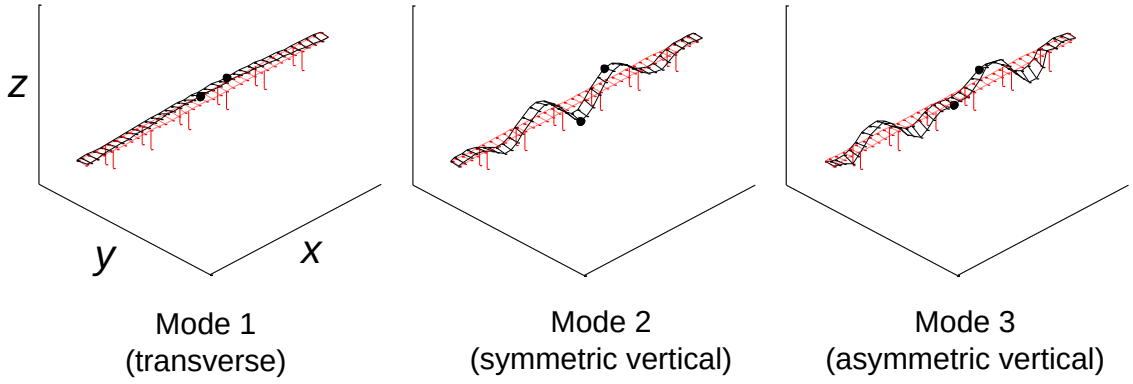

Figure 7. Identified mode shapes (MPV) of Footbridge. The two reference sensor locations are indicated by a heavy dot. Data of the reference sensor on the right is used in the example

Figure 8 to **Figure 10** show the ratio of posterior c.o.v. for Mode 1 to 3, presented in a manner analogous to Figure 5. For each mode, the different values of modal s/n ratio among the points result from the different calculated MPVs of the modal parameters. The

approximation of the first order law is good for Mode 1 (**Figure 8**), but less so for Mode 2 (**Figure 9**) and Mode 3 (**Figure 10**), although in terms of order of magnitude the latter are still acceptable. The poor approximation could be due to a number of reasons, although it is difficult to verify at this stage, e.g., modeling error due to colored excitation (human excitation).

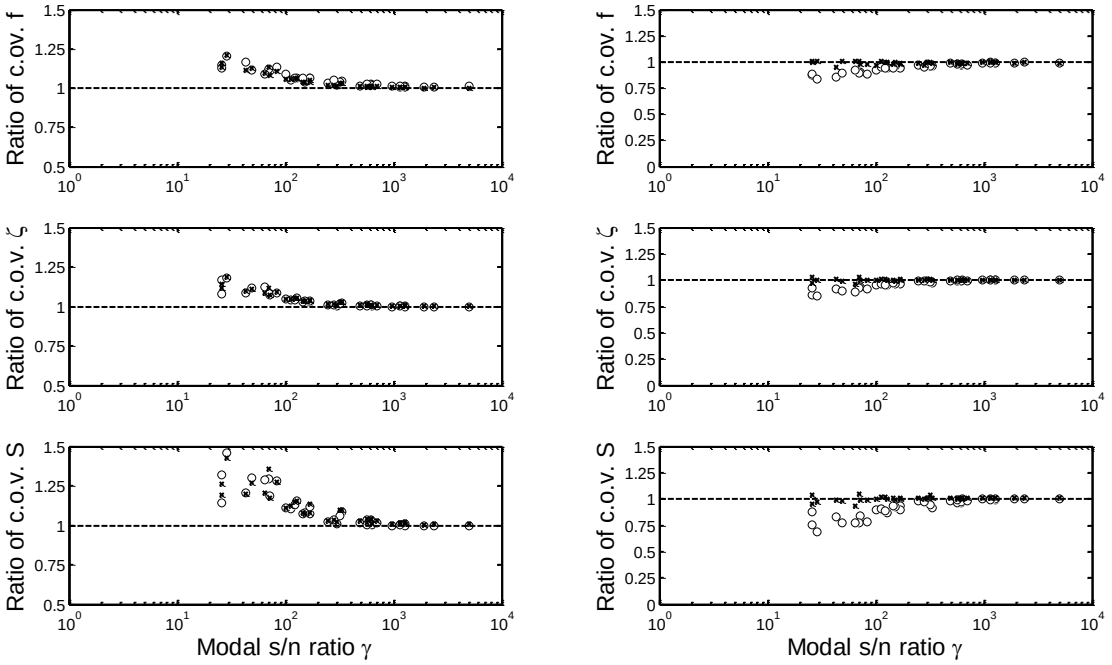

(a) Posterior c.o.v./zeroth order law (b) Posterior c.o.v./exact

Figure 8. Ratio of posterior c.o.v., Footbridge, Mode 1, 37 sets. Same legend as Figure 4

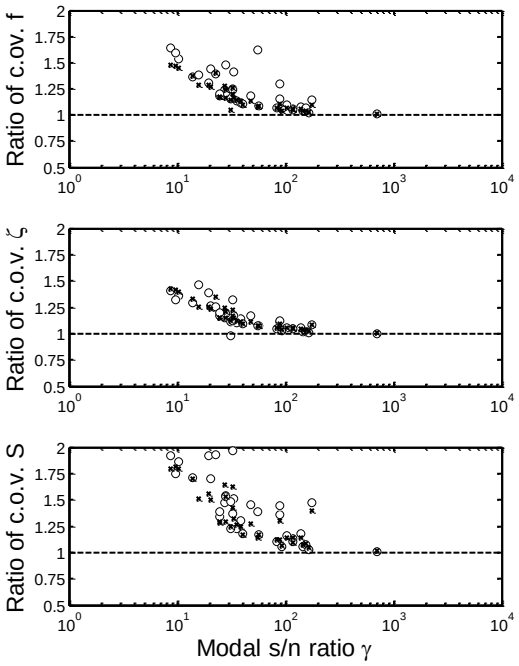

(a) Posterior c.o.v./zeroth order law

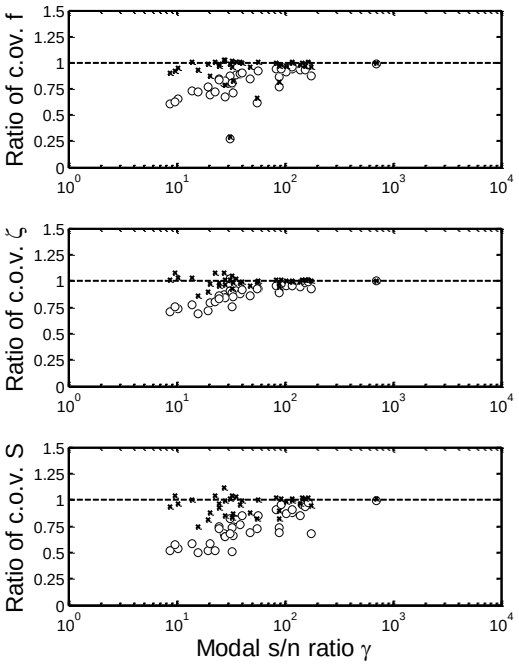

(b) Posterior c.o.v./exact

Figure 9. Ratio of posterior c.o.v., Footbridge, Mode 2, 37 sets. Same legend as Figure 4

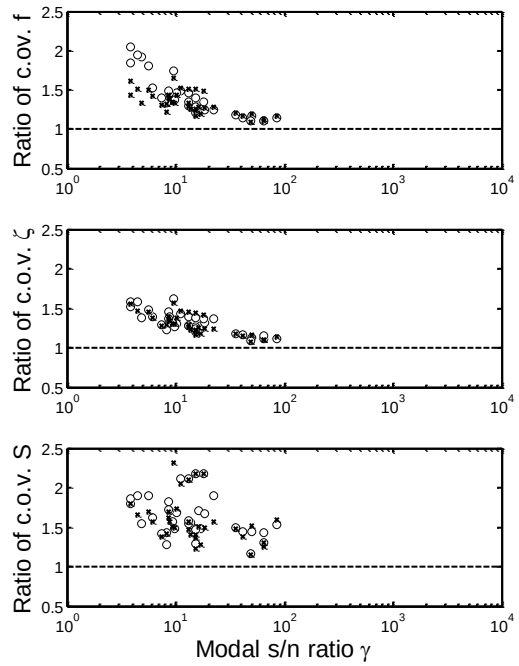

(a) Posterior c.o.v./zeroth order law

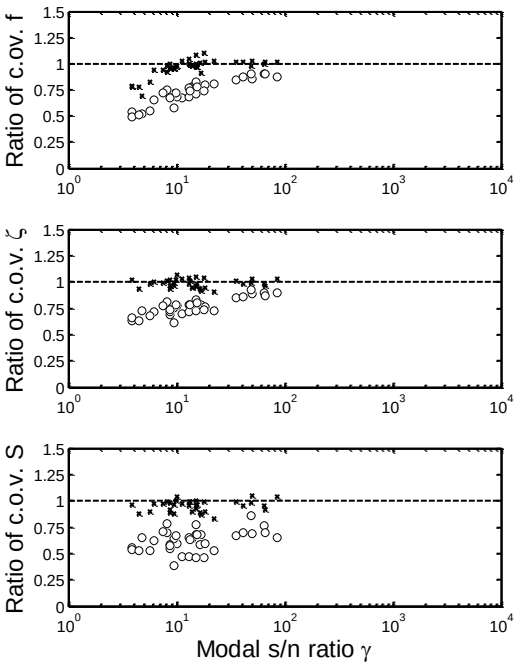

(b) Posterior c.o.v./exact

Figure 10. Ratio of posterior c.o.v., Footbridge, Mode 3, 37 sets. Same as Figure 4

8.3. Statistics summary

Figure 11 shows the posterior c.o.v.s based on the uncertainty laws versus the exact values for all the cases with experimental data. Results for a super-tall building are also reported. The structure was used previously to investigate the zeroth order laws [30]. Although not directly relevant, its modal force PSD identified from measurement was also compared with wind tunnel prediction [36]. The results for the super-tall building presented here were based on 18 hours of acceleration data collected at 50 Hz from a triaxial servo-accelerometer placed on the roof on a normal day. Modal identification was performed on the eleven modes below 3 Hz for each of the thirty six 30 minutes long non-overlapping segments.

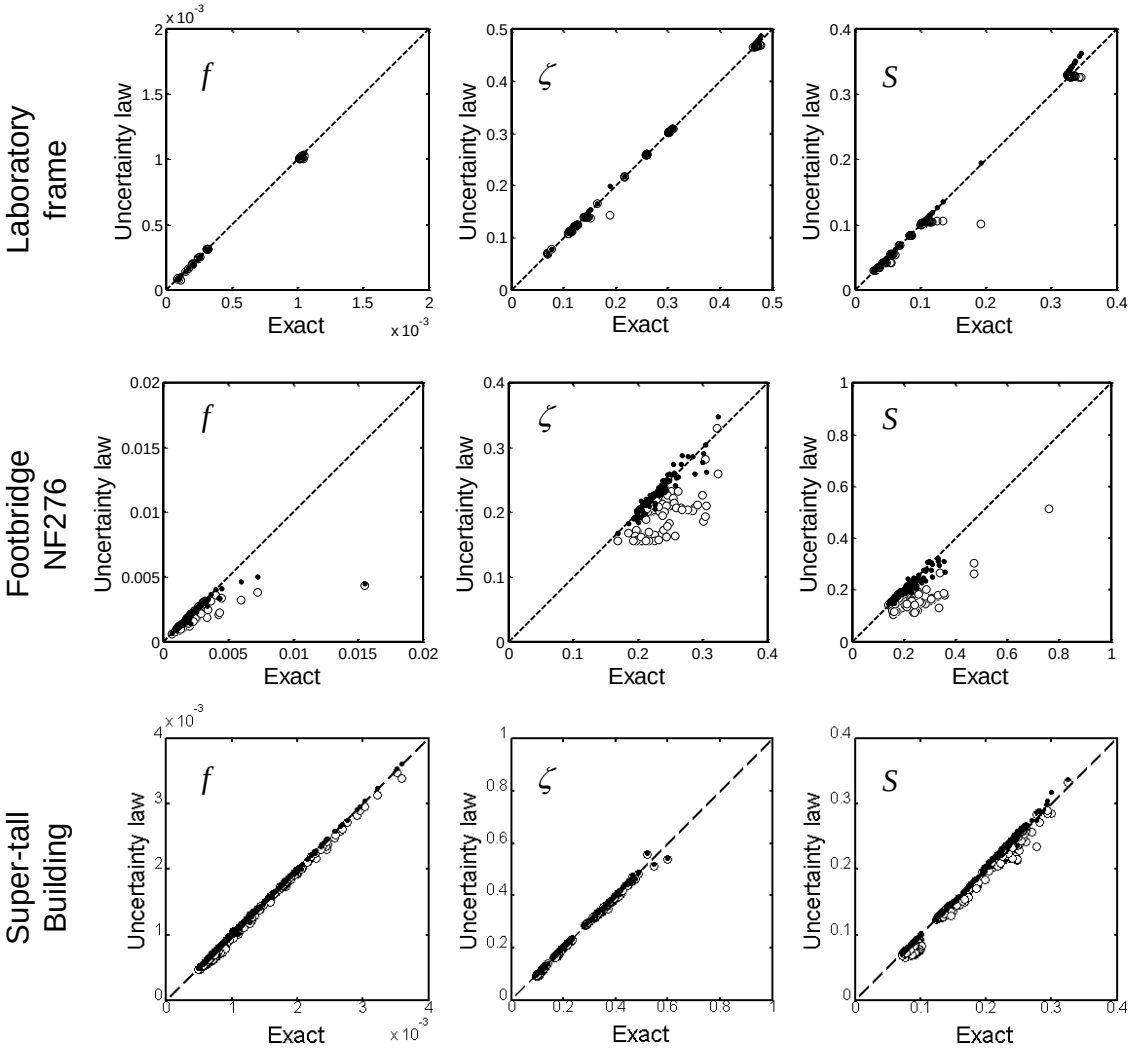

Figure 11. Uncertainty law vs exact values in examples with experimental/field data. Circle – zeroth order law; dot – first order law

Generally the first order uncertainty laws give a reasonable approximation. Table 1 shows the statistics of the identified values (MPV) of the channel noise PSD S_e, the modal force PSD S and the n/e ratio $\nu = S_e / S$ for the field structures. It is presented to give an idea of the order of magnitude of these quantities in the actual field situation.

Table 1. Statistics of S_e, S (MPV) and ν in field structures (one triaxial accelerometer)

Case	Mode	S_e $[(\mu g)^2/Hz]$			S $[(\mu g)^2/Hz]$			$\nu = S_e / S$		
		Min	Mean	Max	Min	Mean	Max	Min	Mean	Max
Footbridge	1	0.16	4.7	25	0.15	0.45	0.97	0.49	11	50
	2	76	152	305	0.09	2.1	11	7.3	206	851
	3	41	143	314	0.08	1.5	6.1	30	156	515
Super-tall building	1	68	301	977	4.0	19	61	5.2	17	41
	2	44	208	501	4.6	19	61	6.2	13	36
	3	0.81	2.3	7.9	0.12	0.43	1.2	3.0	5.5	11
	4	0.36	0.85	2.1	0.21	0.60	1.5	0.79	1.5	2.5
	5	0.58	2.4	6.4	0.10	0.37	0.97	4.2	6.7	11
	6	0.32	1.6	6.2	0.02	0.08	0.21	10	19	36
	7	0.08	0.32	1.0	0.01	0.11	0.89	1.1	4.0	7.0
	8	0.08	1.1	3.8	0.004	0.02	0.12	9.6	50	136
	9	0.29	2.4	10	0.01	0.10	0.61	16	31	55
	10	0.14	2.2	7.3	0.002	0.03	0.11	51	74	99
	11	0.09	1.2	3.8	0.007	0.06	0.29	11	20	31

9. Practical guidelines

In this section we apply the uncertainty laws to produce practical guidelines for planning ambient vibration tests, which is the original motivation of this work. Focus is on the damping ratio, which is the most critical (highest uncertainty) among other modal parameters as well as having the greatest impact in practice due to high sensitivity of predicted response to damping. We will first discuss the bandwidth factor and modal s/n ratio, whose assumptions are inevitable when applying the uncertainty laws at the planning stage. After that we will discuss how to assess test configuration based on simple charts developed from the uncertainty laws.

9.1. Bandwidth factor

The bandwidth factor κ appears in the expressions of the uncertainty laws, e.g., the data length factor B_ζ and the first order coefficient a_ζ. It is a dimensionless quantification of the bandwidth that can be utilized for identifying the subject mode. In the derivation of uncertainty laws, it has been implicitly assumed that in the selected band $f(1\pm\zeta\kappa)$ the mode dominates, or roughly speaking, is within the band where the mode can be seen in the singular value spectrum. It is rational to have κ as large as possible while keeping modeling error risk low. When the modal s/n ratio γ is high the choice of κ is governed by the need to control modeling error risk (e.g., existence of other modes), e.g., by setting an upper limit $\kappa_{\max}$. When γ is not high the choice of κ will depend on γ because the resonance band does. In particular, the two values of frequency ratio β where the modal acceleration PSD SD ($D=[(1-\beta^2)^2+(2\zeta\beta)^2]^{-1}$) equals the noise PSD S_e are given by (recalling $\upsilon = S_e / S$)

$$\beta = \sqrt{\frac{1-2\zeta^2 \pm \sqrt{\upsilon^{-1}-4\zeta^2(1-\zeta^2)}}{1-\upsilon^{-1}}} \tag{31}$$

For small ζ and small υ^{-1} (relevant when γ is not high), this expression implies asymptotically $\kappa \sim \sqrt{\gamma-1}$ (recall $\gamma = 1/4\upsilon\zeta^2$). In practice the band is often selected such that the data PSD $SD+S_e$ has dropped to a level near the noise PSD S_e. This results in a wider band, for which $\kappa = 2\sqrt{\gamma}$ is empirically found to be a reasonable choice.

In summary, for planning purpose the following simple rule is recommended:

$$\kappa = \min(2\sqrt{\gamma}, \kappa_{\max}) \tag{32}$$

This is illustrated in Figure 12(a) for a 1 Hz mode with 1% damping and taking $\kappa_{\max}=10$ to control modeling error risk. Figure 12(b) illustrates the acceleration data PSD and the selected bands based on (32) for different values of γ.

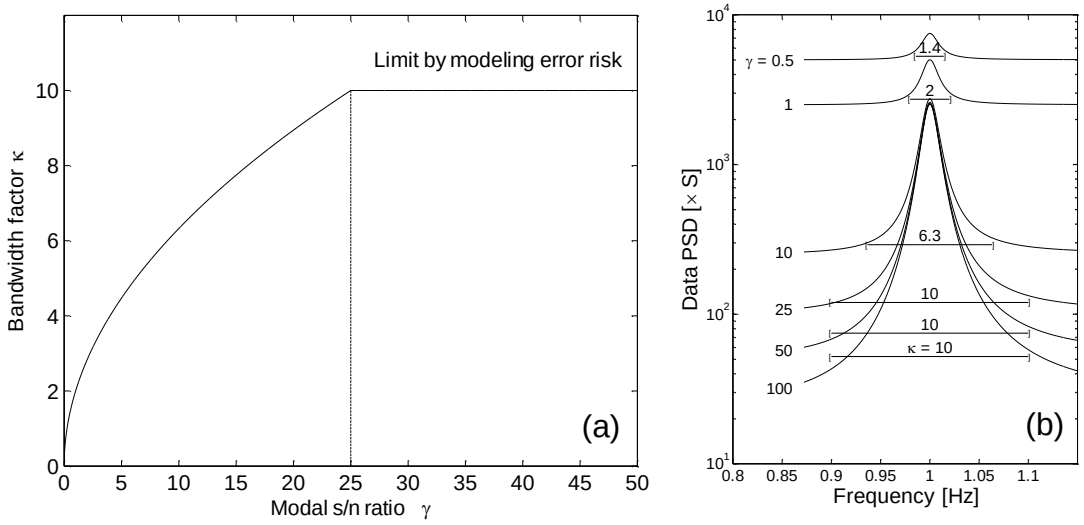

Figure 12 Bandwidth factor κ for planning, assuming a 1 Hz mode with 1% damping and $\kappa_{\max} = 10$ to control modeling error risk

9.2. Modal s/n ratio

The modal s/n ratio γ may be assessed based on experience for situations or more explicitly based on ζ, S_e and S. The damping ratio depends on the type of structure and vibration level, with typical values between 0.5% and 5%. The channel noise PSD S_e depends on the quality of sensors and the data acquisition system (DAQ, comprising cables, digitizing hardware, etc.). The value of S_e can range from the order of 1 $(\mu g)^2 / Hz$ for servo-accelerometers (with appropriate DAQ) to $10^5 (\mu g)^2 / Hz$ for MEMS accelerometers data on smart phones. The modal force PSD S depends on the environmental excitation and the measured DOFs. Simple formulas can be developed in the future to assess its order of magnitude for different types of structures and under different environments (e.g., wind, micro-tremor, traffic). A pre-test or such experience certainly helps. Drawing on experience of the authors, on a normal day (e.g., no strong wind) S may range between 0.01 to 10 $(\mu g)^2 / Hz$ for a single DOF suitably placed for the mode. It can be increased by putting more sensors but the rate depends on the mode shape value of the additional measured DOFs (Section 5).

9.3. Assessing test configuration

Focusing on the damping ratio, the adequacy of a test configuration can be assessed based on charts similar to those in Figure 13. The first order law of posterior c.o.v. for damping ratio is separated into two terms

$$\delta_{\zeta 1} = A_1 A_2 \qquad A_1 = \frac{1}{\sqrt{2\pi\zeta N_c}} \qquad A_2 = \sqrt{\frac{1+a_\zeta/\gamma}{B_\zeta}} \tag{33}$$

so that A_1 and A_2 independently account for the effect of duration (in terms of N_c) and modal s/n ratio (related to channel noise and measured DOFs), respectively. Note that $A_2 = 1$ for $B_\zeta = 1$ and $\gamma \to \infty$, in which case $\delta_{\zeta 1} = A_1$. The term A_1 can thus be interpreted as an optimistic value of identification uncertainty that ignores possible inflation due to finite s/n ratio and limited bandwidth. In the expression of A_2, the values of B_ζ in (8) and a_ζ in (15) are evaluated with κ taken as the minimum of $2\sqrt{\gamma}$ and $\kappa_{\max}$ (see (32) and Figure 12). A low value of $\kappa_{\max}$ reflects anticipation of a challenging mode or risk aversion towards modeling error in the frequency-domain neighborhood of the mode. Note that A_2 is insensitive to γ for $\gamma > 100$ (say), which quantifies a 'sufficiently high modal s/n ratio' where improving equipment has no significant reduction on identification uncertainty (of damping ratio).

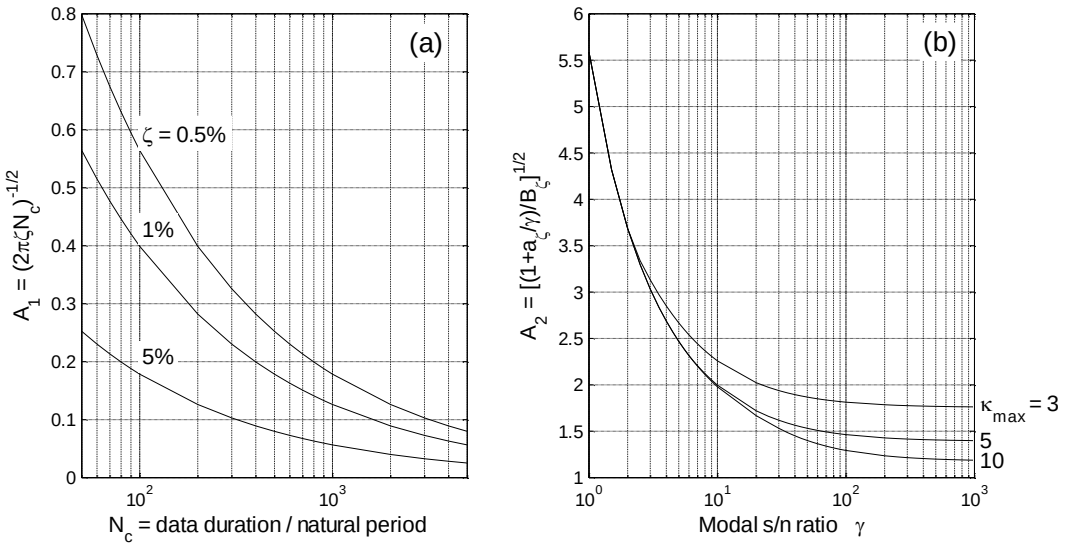

Figure 13 Charts for assessing test configuration. (a) for data duration and (b) for modal s/n ratio

9.4. Example

An example is given to illustrate the use of uncertainty laws for test planning. Consider a super-tall building whose fundamental translational mode has a natural frequency of $f = 0.2$ Hz and a damping ratio of $\zeta = 1\%$. Clearly, these (and other) properties are not known prior to testing but assumptions of their values as well as statistically stationary data are inevitable at the planning stage. The fundamental mode is often the most demanding in data duration because it has the longest period. Consider a trial duration of $N_c = 300$ natural periods, i.e., 1500 sec. Then $A_1 = 1/\sqrt{2\pi(0.01)(300)} = 0.230$, which can also be read approximately from Figure 13(a). This value of c.o.v. is optimistic as it has not accounted for instrument noise and limited bandwidth. Suppose we place a triaxial servo-accelerometer with $S_e = 1(\mu g)^2 / Hz$ at one corner on the roof. Based on experience it gives on a normal day a modal force PSD of $S = 0.1(\mu g)^2 / Hz$. Then ν = 1/0.1 = 10 and $\gamma = 1/4(10)(0.01)^2$ = 250. This value of γ is sufficiently high (in the flat region of A_2 in Figure 13(b)), i.e., equipment (sensor/DAQ quality and sensor number) is good enough. Take $\kappa_{\max} = 10$. Then $\kappa = \min(2\sqrt{250}, 10) = 10$, i.e., choice of band is likely to be governed by modeling error risk control. This gives $B_\zeta \approx 0.724$ (from (8)), $a_\zeta \approx 20.9$ (from (15)) and $A_2 = \sqrt{(1 + 20.9/250)/0.724} = 1.22$ (from (33)), which can also be read approximately from Figure 13(b). Thus, due to instrument noise and limited band, there is a 22% inflation of identification uncertainty and consequently $\delta_{\zeta 1} = 0.230 \times 1.22 = 28\%$, which is acceptable. It may not be necessary to further reduce the identification uncertainty, but otherwise lengthening the data duration is the only effective means. Adding sensors or further reducing the channel noise will have little or no effect.

Suppose now the sensor or DAQ has lower quality, in the sense that $S_e = 100(\mu g)^2 / Hz$. Using the same trial duration of $N_c = 300$ gives $A_1 = 0.230$ the same as before. To

assess instrument effect, $\nu = 100/0.1 = 1000$ and $\gamma = 1/(4)(1000)(0.01)^2 = 2.5$ (quite low). The usable bandwidth is $\kappa = \min(2\sqrt{2.5}, 10) = 3.16$, i.e., governed by resonance band. This gives $B_\zeta \approx 0.344$, $a_\zeta \approx 6.85$ and $A_2 = \sqrt{(1+6.85/2.5)/0.344} = 3.29$. There is thus over 200% inflation due to (poor) instrument (which also narrows the usable band), giving $\delta_{\zeta 1} = 0.230 \times 3.29 = 76\%$, which is not acceptable. From Figure 13(b), A_2 is quite sensitive to γ around 2.5 and so identification uncertainty can be effectively reduced by increasing γ. This is explored next by improving the quality of sensor/DAQ or increasing the number of measured DOFs.

For example, reducing the channel noise S_e from 100 to 10 $(\mu g)^2 / Hz$ reduces ν to 100 and increases γ to 25. The usable band is $\kappa = \min(2\sqrt{25}, 10) = 10$, for which $B_\zeta \approx 0.724$, $a_\zeta \approx 20.9$ and $A_2 = \sqrt{(1+20.9/25)/0.724} = 1.59$. There is only an inflation of 59% of uncertainty now, giving $\delta_{\zeta 1} = 0.230 \times 1.59 = 37\%$ (down from 76% before). Further reducing S_e to $1\,(\mu g)^2 / Hz$ can bring $\delta_{\zeta 1}$ down to 28%, whose effect is marginal.

Alternatively, suppose we keep using the same sensor and DAQ, i.e., S_e remains at 100 $(\mu g)^2 / Hz$, but now we install additional triaxial sensors at other corners on the roof. Since the mode shape values at other corners is similar to the existing ones, the modal force PSD S increases roughly linearly with the number of sensors. Suppose we put another three sensors at the remaining three corners of the roof. This will increase S by four times from 0.1 to $0.4\,(\mu g)^2 / Hz$ and hence γ from 2.5 to 10. The usable band is $\kappa = \min(2\sqrt{10}, 10) = 6.32$, for which $B_\zeta \approx 0.595$, $a_\zeta \approx 13.3$, $A_2 = \sqrt{(1+13.3/10)/0.595} = 1.97$ and $\delta_{\zeta 1} = 0.230 \times 1.97 = 45\%$. The addition of three sensors roughly reduces identification uncertainty by half, although it may still be considered unacceptable. Without further adding sensors, the identification uncertainty

can be reduced by increasing the data duration. Doubling the duration from 300 to 600 natural periods reduces the posterior c.o.v. to $1/\sqrt{2}$ of its original value (i.e., by about 30%) to $45\%/\sqrt{2} = 32\%$, which may be acceptable. The resulting data duration is (5)(600) = 3000 sec (about an hour). One needs to check the data to see whether stationary assumption is still justified. This is especially relevant for the damping ratio and the modal force PSD.

10. Conclusions

Beyond the current state-of-the-art in operational modal analysis, this work has discovered the fundamental relationship between the identification uncertainty of modal parameters and testing configuration. A Bayesian approach has been adopted to establish results that are consistent with probability and structural dynamics. The first order uncertainty laws (see (13)) allow one to account for the effects of test configuration when planning ambient vibration tests. The theory reveals the remarkable fact that the apparently complicated effect of *test configuration on identification uncertainty can be fundamentally encapsulated in the modal s/n ratio*. This is related to the channel noise, environmental excitation and measured DOFs. The mathematical correctness and quality of approximation of the first order laws under non-asymptotic conditions have been verified with synthetic data and experimental data under laboratory and field environment.

A quick remark on the required quality and number of sensors is in order. To obtain a mode shape at more locations obviously requires more sensors. Otherwise, improving the accuracy of modal properties (other than mode shape) is not a good justification for deploying more sensors. One is likely to either have good enough modal s/n ratio or it would not help with just a few more sensors. The modal s/n ratio can be sufficiently high with only one or two good and suitably placed sensors. Otherwise, a material reduction in identification uncertainty would require an order of magnitude increase in the modal s/n ratio and hence the number of sensors. Thus, a structural health monitoring system with only one or two good accelerometers can give practically the same accuracy for natural frequency or damping as another one with hundreds. If the sensors have high noise, they

are simply not fit for the purpose and should be substituted by better ones. It is not advised to make up quality with quantity.

11. Acknowledgments

This work is funded by the UK Engineering and Physical Sciences Research Council (EP/N017897/1 & EP/N017803/1). The support is gratefully acknowledged.

12. References

[1] B. Peeters, G. De Roeck, Stochastic system identification for operational modal analysis: a review, Journal of Dynamical Systems, Measurement, and Control, 123 (2001) 659-667.

[2] R. Brincker, P.H. Kirkegaard (Eds), Special issue on operational modal analysis, Mechanical Systems and Signal Processing, 24(5) (2010) 1209-1604.

[3] R. Brincker, C. Ventura, Introduction to Operational Modal Analysis, Wiley, London, 2015.

[4] L. Hermans and H. Van der Auweraer, Modal testing and analysis of structures under operational conditions: industrial applications, Mechanical Systems and Signal Processing, 13(2) (1999) 193-216.

[5] S.S. Ivanovic, M.D. Trifunac, M.L. Todorovska, Ambient vibration tests of structures – a review, ISET Journal of Earthquake Technology, 37(4) (2000) 165 – 197.

[6] J.M.W. Brownjohn, A. De Stefano, Y.L. Xu, H. Wenzel, A.E. Aktan, Vibration-based monitoring of civil infrastructure: challenges and successes, Journal of Civil and Structural Health Monitoring, 1 (2011) 79-95.

[7] H. Wenzel, D. Pichler, Ambient vibration monitoring, Wiley, UK, 2005.

[8] S. Alampalli, Effects of testing, analysis, damage, and environment on modal parameters, Mechanical Systems and Signal Processing, 14(1) (2000) 63-74.

[9] J.M. Ko, J.Y. Wang, Y.Q. Ni, K.K. Chak, Observation on environmental variability of modal properties of a cable-stayed bridge from one-year monitoring data, In:

Chang FK, editor. Structural health monitoring: from diagnostics and prognostics to structural health management. Lancaster (PA): DEStech. p. 467–74, 2003.

[10] J.T. Kim, C.B. Yun, J.H. Yi, Temperature effects on modal properties and damage detection in plate-girder bridges, In: Chang FK, Yun CB, Spencer Jr BF, editors. Advanced smart materials and structures technology. Lancaster (PA): DEStech; 504–511, 2004.

[11] G.C. Goodwin, R.L. Payne, Dynamic system identification: experiment design and data analysis. London: Academic Press, 1977.

[12] P.H. Kirkegaard, R. Brincker, On the optimal locations of sensors for parametric identification of linear structural systems, Mechanical Systems and Signal Processing, 8 (1994) 639–47.

[13] C. Papadimitriou, Optimal sensor placement methodology for parametric identification of structural systems, Journal of Sound and Vibration, 278 (4-5) (2004), 923-947.

[14] C. Cappello, D. Sigurdardottir, B. Glisic, D. Zonta and M. Pozzi, On predicting monitoring system effectiveness, Proc. SPIE 9435, Sensors and Smart Structures Technologies for Civil, Mechanical, and Aerospace Systems 2015, 94352M (March 27, 2015); doi:10.1117/12.2086365.

[15] R.T. Cox, The Algebra of Probable Inference, Johns Hopkins, Baltimore, 1961.

[16] E.T. Jaynes, Probability Theory: The Logic of Science. Cambridge University Press, UK, 2003.

[17] J.L. Beck, Bayesian system identification based on probability logic, Structural Control and Health Monitoring, 17 (7) (2010) 825–847.

[18] K.V. Yuen and L.S. Katafygiotis, Bayesian Fast Fourier Transform approach for modal updating using ambient data, Advances in Structural Engineering, 6 (2) (2003) 81-95.

[19] S.K. Au, F.L. Zhang and Y.C. Ni, Bayesian operational modal analysis: theory, computation, practice, Computers and Structures, 126 (2013) 3-14.

[20] F.L. Zhang, Y.Q. Ni, Y.C. Ni, Mode identifiability of a cable-stayed bridge based on a Bayesian method, Smart Structures and Systems 17(3) (2016) 471-489.

[21] Y.C. Ni, X.L. Lu, W.S. Lu, Field dynamic test and Bayesian modal identification

of a special structure-the palms together dagoba, Structural Control and Health Monitoring 23(5) (2016) 838-856.

[22] F.L. Zhang, H.B. Xiong, W.X. Shi, X. Ou, Structural health monitoring of a super tall building during different stages using a Bayesian approach, Structural Control and Health Monitoring (2016) DOI: 10.1002/stc.1840.

[23] H.F. Lam, J. Hu, J.H. Yang, Bayesian operational modal analysis and Markov chain Monte Carlo-based model updating of a factory building, Engineering Structures 132 (2017) 314-336.

[24] P. Liu, F.L. Zhang, P.Y. Lian, Dynamic characteristic analysis of two adjacent multi-grid composite wall structures with a seismic joint by a Bayesian approach. Journal of Earthquake Engineering 20(8) (2016) 1295-1321.

[25] R. Pintelon, P. Guillaume and J. Schoukens, Uncertainty calculation in (operational) modal analysis, Mechanics Systems and Signal Processing, 21 (2007) 2359-2373.

[26] E. Reynders, R. Pintelon and G. De Roeck, Uncertainty bounds on modal parameters obtained from stochastic subspace identification, Mechanical Systems and Signal Processing, 22 (2007), 948–969.

[27] T. Matarazzo and S. Pakzad, Sensitivity Metrics for Maximum Likelihood System Identification, ASCE-ASME J. Risk Uncertainty Eng. Syst., Part A: Civil Engineering, DOI: 10.1061/AJRUA6.0000832.

[28] K. Ciloglu, Y. Zhou, F. Moon and A. Aktan, Impacts of Epistemic Uncertainty in Operational Modal Analysis, Journal of Engineering Mechanics, 138(9) (2012) 1059-1070.

[29] S. K. Au, Uncertainty laws in ambient modal identification. Part I: theory, Mechanical Systems and Signal Processing, 48(1-2) (2014) 15-33.

[30] S.K. Au, Uncertainty laws in ambient modal identification. Part II: implications and field verification, Mechanical Systems and Signal Processing, 48 (2014) 1-2, 34-48.

[31] D.R. Brillinger, Time series: Data analysis and theory, Holden-Day, Inc., San Francisco, 1981.

[32] S.K. Au, Fast Bayesian FFT method for ambient modal identification with separated modes, Journal of Engineering Mechanics, ASCE, 137 (3) (2011) 214-226.

[33] F.L. Zhang, S.K. Au, Fundamental two-stage formulation for Bayesian system identification. Part II: Ambient modal identification, Mechanical Systems and Signal Processing, 66-67 (2016) 43-61.

[34] S.K. Au and F.L. Zhang, Fast Bayesian ambient modal identification incorporating multiple setups, Journal of Engineering Mechanics, 138(7) (2012) 800-815.

[35] F.L. Zhang, S.K. Au, H.F. Lam, Assessing uncertainty in operational modal analysis incorporating multiple setups using a Bayesian approach, Structural Control and Health Monitoring, 22(3) (2015) 395-416.

[36] S.K. Au and P. To, Full-scale validation of dynamic wind load on a super-tall building under strong wind, Journal of Structural Engineering, ASCE, 138(9) (2012) 1161-1172.

13. Appendix. First order Asymptotics of second derivatives of NLLF

In this section we derive the first order asymptotic expressions for the derivatives $L^{(ff)}$, $L^{(\zeta\zeta)}$, $L^{(SS)}$ and $L^{(\zeta S)}$ w.r.t. $\gamma^{-1} = 4\nu\zeta^2$ for $N_f \to \infty$ and $\zeta \to 0$. We first consider asymptotics for $N_f \to \infty$, which leads to expressions that involve sums over the selected frequency band. Further asymptotics for $\zeta \to 0$ leads to the final analytical expressions for the sums. To facilitate analysis we separate the NLLF in (4) into a log-determinant term and a quadratic term, i.e., $L = L_D + L_Q$ where

$$L_D = nN_f \ln \pi + (n-1)N_f \ln S_e + \sum_k \ln(SD_k + S_e) \tag{34}$$

$$L_Q = S_e^{-1}[d - \sum_k (1 + \frac{S_e}{SD_k})^{-1} d_k] \qquad d_k = \overline{\mathbf{\Phi}}^T \mathbf{D}_k \overline{\mathbf{\Phi}} \tag{35}$$

13.1. Long data asymptotics

We first prove the following expressions which are asymptotically correct for $N_f \to \infty$:

$$L^{(ff)} \sim \sum_k D_k^2 (D_k^{-1})^{(f)2} (1 + e_k)^{-2} \tag{36}$$

$$L^{(\zeta\zeta)} \sim \sum_k D_k^2 (D_k^{-1})^{(\zeta)2} (1 + e_k)^{-2} \tag{37}$$

$$L^{(SS)} \sim S^{-2} \sum_k (1 + e_k)^{-2} \tag{38}$$

$$L^{(\zeta S)} \sim -S^{-1} \sum_k D_k (D_k^{-1})^{(\zeta)} (1 + e_k)^{-2} \tag{39}$$

where

$$e_k = \frac{S_e}{SD_k} \tag{40}$$

The terms $(D_k^{-1})^{(f)}$ and $(D_k^{-1})^{(\zeta)}$ are the derivatives of $D_k^{-1} = (1 - \beta_k^2)^2 + (2\zeta\beta_k)^2$ w.r.t. f and ζ, respectively. Direct differentiation gives

$$(D_k^{-1})^{(f)} = 4f^{-1}\beta_k^2(\beta_k^2 - 1 + 2\zeta^2) \qquad (D_k^{-1})^{(\zeta)} = 8\zeta\beta_k^2 \tag{41}$$

13.1.1. Expressions for $L^{(ff)}$ and $L^{(\zeta\zeta)}$

First consider $L_D^{(ff)}$. Differentiating (34) w.r.t. f and simplifying gives

$$L_D^{(f)} = \sum_k (SD_k + S_e)^{-1} SD_k^{(f)} \tag{42}$$

$$L_D^{(ff)} = -\sum_k (1+e_k)^{-2} D_k^{-2} D_k^{(f)2} + \sum_k (1+e_k)^{-1} D_k^{-1} D_k^{(ff)} \tag{43}$$

We next express $L_D^{(ff)}$ in terms of the derivatives of D_k^{-1} as they are easier to analyze.

The derivatives of D_k are related to those of D_k^{-1} by

$$D_k^{(f)} = -D_k^2 (D_k^{-1})^{(f)} \qquad D_k^{(ff)} = 2D_k^3 (D_k^{-1})^{(f)2} - D_k^2 (D_k^{-1})^{(ff)} \tag{44}$$

Substituting into (43) gives, after algebra,

$$L_D^{(ff)} = \sum_k D_k^2 (D_k^{-1})^{(f)2} (1+e_k)^{-2} (1+2e_k) - \sum_k D_k (D_k^{-1})^{(ff)} (1+e_k)^{-1} \tag{45}$$

For the derivatives of L_Q, differentiating (35) w.r.t. f and simplifying gives

$$L_Q^{(f)} = \sum_k (1 + \frac{S_e}{SD_k})^{-2} S^{-1} (D_k^{-1})^{(f)} d_k \tag{46}$$

$$L_Q^{(ff)} = -2\sum_k (1+e_k)^{-3} S_e S^{-2} (D_k^{-1})^{(f)2} d_k + \sum_k (1+e_k)^{-2} S^{-1} (D_k^{-1})^{(ff)} d_k \tag{47}$$

Equation (47) depends on $\{d_k\}$, which in turn depends on the FFT data $\{\mathcal{F}_k\}$. The latter is unknown prior to data collection. For the purpose of deriving uncertainty laws, it is modeled by a stochastic process consistent with the identification model. By a similar argument in Section 4.2 of [29], it can be shown that for any positive deterministic sequence $\{c_k\}$,

$$\sum_k c_k d_k \sim \sum_k c_k (SD_k + S_e) \qquad N_f \to \infty \tag{48}$$

where the modal parameters involved on the RHS represent the MPV, which are asymptotically the same as the actual properties that result in the data (assuming no modeling error). Evaluating (47) at the MPV and applying (48) gives, as $N_f \to \infty$,

$$\begin{aligned} L_Q^{(ff)} \sim & -2\sum_k (1+e_k)^{-3} S_e S^{-2} (D_k^{-1})^{(f)2} (SD_k + S_e) \\ & + \sum_k (1+e_k)^{-2} S^{-1} (D_k^{-1})^{(ff)} (SD_k + S_e) \end{aligned} \tag{49}$$

To simplify, note that

$$(1+e_k)^{-1}(SD_k + S_e) = (1+\frac{S_e}{SD_k})^{-1}(SD_k + S_e) = SD_k \tag{50}$$

Using this, (49) can be written as

$$L_Q^{(ff)} \sim -2\sum_k D_k^2 (D_k^{-1})^{(f)2} (1+e_k)^{-2} e_k + \sum_k D_k (D_k^{-1})^{(ff)} (1+e_k)^{-1} \tag{51}$$

Combining (45) and (51) gives (36). Using exactly the same procedure, $L^{(\zeta\zeta)}$ is given by the same expression with f replaced by ζ, as shown in (37).

13.1.2. Expression for $L^{(SS)}$

Differentiating (34) w.r.t. S and simplifying gives

$$L_D^{(S)} = \sum_k (SD_k + S_e)^{-1} D_k \qquad L_D^{(SS)} = -S^{-2} \sum_k (1+e_k)^{-2} \tag{52}$$

On the other hand, differentiating (35) w.r.t. S and simplifying gives

$$L_Q^{(S)} = -\sum_k (1+\frac{S_e}{SD_k})^{-2} D_k^{-1} S^{-2} d_k \qquad L_Q^{(SS)} = 2S^{-2} \sum_k (1+e_k)^{-3} S^{-1} D_k^{-1} d_k \tag{53}$$

Evaluating at the MPV, applying (48) and simplifying gives, as $N_f \to \infty$,

$$L_Q^{(SS)} \sim 2S^{-2} \sum_k (1+e_k)^{-2} \tag{54}$$

Combining (52) and (54) gives (38).

13.1.3. Expression for $L^{(\zeta S)}$

Differentiating $L_Q^{(S)}$ in (52) w.r.t. ζ and simplifying gives

$$L_D^{(\zeta S)} = S_e \sum_k (SD_k + S_e)^{-2} D_k^{(\zeta)} \tag{55}$$

Substituting an analogous expression in (44) for $D_k^{(\zeta)}$ and simplifying gives

$$L_D^{(\zeta S)} = -S^{-1} \sum_k D_k (D_k^{-1})^{(\zeta)} (1+e_k)^{-2} e_k \tag{56}$$

On the other hand, differentiating $L_Q^{(S)}$ in (53) w.r.t. ζ and simplifying gives

$$L_Q^{(\zeta S)} = -S^{-2} \sum_k (D_k^{-1})^{(\zeta)} (1+e_k)^{-3} (1-e_k) d_k \tag{57}$$

Evaluating at the MPV, applying (48) and simplifying using (50) gives, as $N_f \to \infty$,

$$L_Q^{(\zeta S)} \sim -S^{-1} \sum_k D_k (D_k^{-1})^{(\zeta)} (1+e_k)^{-2} (1-e_k) \tag{58}$$

Combining (56) and (58) gives (39).

13.2. Small damping asymptotics

Equations (36) to (39) are asymptotic expressions for $N_f \to \infty$ and they are applicable for general value of ζ. They involve sums that carry limited insights. We next consider their asymptotic behavior for $\zeta \to 0$, which implies large D_k and small e_k. The strategy is to make use of the Taylor expansion of $(1+e_k)^{-2}$ for small e_k:

$$(1+e_k)^{-2} = 1 - 2e_k + 3e_k^2 - 4e_k^3 + \ldots \tag{59}$$

We will outline derivation for $L^{(ff)}$, which leads to the coefficient c_{ff} in (26). The expressions for $L^{(\zeta\zeta)}$, $L^{(SS)}$ and $L^{(\zeta S)}$ can be obtained similarly (details omitted), leading to the coefficients $c_{\zeta\zeta}$, c_{SS} and $c_{\zeta S}$ in (26) and (27).

Keeping up to the first order term in (59), substituting into (36) and using $D_k e_k = \nu$,

$$L^{(ff)} \sim \sum_k D_k^2 (D_k^{-1})^{(f)2} (1-2e_k) = \sum_k D_k^2 (D_k^{-1})^{(f)2} - 2\nu \sum_k D_k (D_k^{-1})^{(f)2} \qquad (60)$$

Substituting $(D_k^{-1})^{(f)}$ from (41) into (60) leads to sums of the form $\sum_k D_k^a (\beta_k - 1)^b$. A technique similar to that in Appendix II of [29] is used to analyze this sum, except that the next order term should also be retained in addition to the leading order term. Omitting algebra, the result reads

$$L^{(ff)} \sim L_0^{(ff)} + L_1^{(ff)} \qquad (61)$$

where $L_0^{(ff)}$ is the zeroth (leading) order term in (22); and

$$L_1^{(ff)} = -64 f^{-2} N_c \nu\zeta (\kappa - \tan^{-1}\kappa) \qquad (62)$$

is the first order term. This gives

$$\frac{L_1^{(ff)}}{L_0^{(ff)}} = \frac{-64 f^{-2} N_c \nu\zeta (\kappa - \tan^{-1}\kappa)}{4 f^{-2} N_c \zeta^{-1} [\tan^{-1}\kappa - \kappa/(\kappa^2+1)]} = -\left[\frac{4(\kappa - \tan^{-1}\kappa)}{\tan^{-1}\kappa - \kappa/(\kappa^2+1)}\right](4\nu\zeta^2) \qquad (63)$$

Since $\gamma^{-1} = 4\nu\zeta^2$, we can write $L^{(ff)} \sim L_0^{(ff)}(1 - c_{ff}\gamma^{-1})$ as in (25) with c_{ff} given by (26).